



# Identifying metabolic alterations associated with coral growth anomalies using $^1\text{H}$ NMR metabolomics

Erik R. Andersson<sup>1,2</sup> · Rusty D. Day<sup>1,2,3</sup> · Thierry M. Work<sup>4</sup> · Paul E. Anderson<sup>5</sup> · Cheryl M. Woodley<sup>6</sup> · Tracey B. Schock<sup>2</sup>

Received: 16 September 2020 / Accepted: 25 May 2021

© The Author(s), under exclusive licence to Springer-Verlag GmbH Germany, part of Springer Nature 2021

**Abstract** Coral growth anomalies (GAs) are tumor-like protrusions that are detrimental to coral health, affecting both the coral skeleton and soft tissues. These lesions are increasingly found throughout the tropics and are commonly associated with high human population density, yet little is known about the molecular pathology of the disease. Here, we investigate the metabolic impacts of GAs through  $^1\text{H}$  nuclear magnetic resonance (NMR) metabolomics in *Porites compressa* tissues from a site of high disease prevalence (Coconut Island, Hawaii). We putatively identified 18 metabolites (8.1% of total annotated features) through complementary  $^1\text{H}$  and  $^1\text{H}$ - $^{13}\text{C}$  heteronuclear single quantum correlation NMR data that increase confidence in pathway analyses and may bolster future coral metabolite annotation efforts. Extract yield was elevated in both GA and unaffected (normal tissue from a diseased colony) compared to reference (normal

tissue from GA-free colony) samples, potentially indicating elevated metabolic activity in GA-impacted colonies. Relatively high variation in metabolomic profiles among coral samples of the same treatment (i.e., inter-colony variation) confounded data interpretation, however, analyses of paired GA and unaffected samples identified 73 features that differed between these respective metabolome types. These features were largely annotated as unknowns, but 1-methylnicotinamide and trigonelline were found to be elevated in GA samples, while betaine, glycine, and histamine were lower in GA samples. Pathway analyses indicate decreased choline oxidation in GA samples, making this a pathway of interest for future targeted studies. Collectively, our results provide unique insights into GA pathophysiology by showing these lesions alter both the absolute and relative metabolism of affected colonies and by identifying features (metabolites and unknowns) and metabolic pathways of interest in GA pathophysiology going forward.

Topic Editor Mark Vermeij

**Supplementary information** The online version contains supplementary material available at <https://doi.org/10.1007/s00338-021-02125-7>.

✉ Erik R. Andersson  
anderssoner@g.cofc.edu

<sup>1</sup> Grice Marine Laboratory, Department of Biology, College of Charleston, 205 Fort Johnson Rd., Charleston, SC 29412, USA

<sup>2</sup> Chemical Sciences Division, National Institute of Standards and Technology, Hollings Marine Laboratory, Charleston, SC 29412, USA

<sup>3</sup> Present Address: Marine Science and Nautical Training Academy (MANTA), 417 Planters Trace Dr, Charleston, SC 29412, USA

**Keywords** Coral disease · Growth anomalies · Metabolomics · NMR spectroscopy · *Porites compressa*

<sup>4</sup> U.S. Geological Survey National Wildlife Health Center, Honolulu Field Station, Honolulu, HI 96850, USA

<sup>5</sup> Department of Computer Science and Software Engineering, California Polytechnic State University, San Luis Obispo, CA 93407, USA

<sup>6</sup> National Oceanic and Atmospheric Administration, National Ocean Service, National Centers for Coastal Ocean Sciences, Hollings Marine Laboratory, Charleston, SC 29412, USA

## Introduction

Coral reefs contain a disproportionately large amount of the ocean's biodiversity and productivity, making them one of the most ecologically and economically important ecosystems in the world (Odum and Odum 1955; Moberg and Folke 1999). Nonetheless, the status of these ecosystems has declined in recent decades due to a combination of local and global challenges (Hughes et al. 2017). Increasing atmospheric carbon dioxide levels pose a ubiquitous threat to coral reefs due to the associated increase in oceanic temperatures and ocean acidification (Hoegh-Guldberg et al. 2007), while chemical pollution, eutrophication, fishing pressure, and other localized stressors also contribute to coral reef degradation (Knowlton 2001; van Dam et al. 2011). Coral disease occurrence is commonly linked to human activity (Green and Bruckner 2000) and is influenced by both local and global stressors, which may shift host–pathogen interactions in favor of disease (Lesser et al. 2007; Burge et al. 2014). Disease outbreaks can devastate impacted coral populations (e.g., Aronson and Precht 2001), and the rising prevalence and impact of coral diseases make them a substantial threat to coral reef health worldwide (Bruckner 2016). Coral diseases often share similar visual indicators, and any given disease may not originate from a single causative agent, thus complicating efforts to define disease pathology (Work and Aeby 2006; Lesser et al. 2007). However, emerging molecular techniques have the potential to improve diagnostic ability by investigating new aspects of coral biology as well as disease pathophysiology and etiology (Pollock et al. 2011).

Coral growth anomalies (GAs) are generally characterized by irregular and accelerated growth of a less dense skeleton resulting in a tumor-like mass on a coral colony, with overlying tissues having fewer polyps, fewer endosymbiotic dinoflagellates (family Symbiodiniaceae), and reduced reproductive potential (Work et al. 2016). Histological descriptions of GAs have shown irregular polyp structure, thickened calcareous layer, and increased cell proliferation with suppressed apoptosis (Domart-Coulon et al. 2006; Yasuda and Hidaka 2012). These lesions affect many coral species and are common across the Indo-Pacific but less common in the Caribbean (Work et al. 2016). GAs do not typically lead directly to coral mortality, but their abnormal characteristics lower the fitness of impacted colonies and they therefore pose an ecological threat to coral populations where prevalence is high (Stimson 2011).

Although the biological and ecological impacts of these lesions have been studied using a wide range of methods (e.g., Domart-Coulon et al. 2006; Burns and Takabayashi

2011; Kelly et al. 2016; Palmer and Baird 2018; Preston and Richards 2021), the cause and pathogenesis of GAs remain unknown. Early theorized causes include ultraviolet radiation (Coles and Seapy 1998; Stimson 2011) and pathogenic microorganisms (Kaczmarzky and Richardson 2007). More recent molecular investigations have produced contradictory results regarding the involvement of oncogenes in GA pathology (Spies and Takabayashi 2013; Zhang et al. 2017; Frazier et al. 2017). To date, conclusive evidence to support any of these hypotheses is lacking; however, the correlation between human population and GA prevalence (Aeby et al. 2011a, 2011b) strongly indicates localized human activities influence GA formation.

The development of molecular biology–omics techniques has facilitated the investigation of biological questions that were previously inaccessible (Joyce and Palsson 2006), and these techniques have recently emerged to supplement more traditional approaches in attempting to determine disease causative agents (Madsen 2005). One such molecular tool is metabolomics, a developing field dedicated to the study of low-molecular-weight compounds (here we refer specifically to the water-soluble polar metabolites) in biological samples under predetermined physiological conditions. These compounds are essential products and intermediates in biochemical pathways that fluctuate with gene expression and enzymatic activities, making the metabolome closely tied to the biochemical phenotype and thus excellent for closely monitoring organismal response to perturbations such as disease (Goodacre 2007; Viant 2008; Bundy et al. 2009). Targeted approaches are generally used in cases where specific, predetermined metabolites are of particular interest (Roberts et al. 2012). In other cases, an untargeted approach is common, where as many metabolites as possible are measured and biological interpretations are made based on the composition and relative abundances of the entire metabolomic profile (Alonso et al. 2015). These studies do not necessarily rely on traditional hypotheses to generate valuable data and biological information. In fact, many untargeted metabolomics studies naturally result in hypothesis formation when unexpected metabolic effects and activities are revealed (Kell and Oliver 2004; Bundy et al. 2009). These characteristics make metabolomics a potentially strong method for progressing our understanding of coral disease pathogenesis.

Applications of metabolomics to study stony corals have been limited by challenges associated with fitting common metabolomic methods to these unique organisms. The coral holobiont presents a complex biological matrix consisting of coral tissues and contiguous skeleton, symbiotic dinoflagellates, and associated microbial communities. Therefore, typical best practices for metabolomics cannot be applied automatically. Accordingly, many coral

metabolomics studies have emphasized methods development and optimization (Gordon et al. 2013; Andersson et al. 2019) or demonstrating the utility of metabolomics in coral research by establishing foundational properties of the coral metabolome (Parkinson and Baums 2014; Sogin et al. 2014, 2017; Hartmann et al. 2017; Lohr et al. 2019b; Vohsen et al. 2019). Nevertheless, metabolomics methods have been used to investigate the impacts of thermal stress and bleaching history (Sogin et al. 2016; Hillyer et al. 2017, 2018; Lohr et al. 2019a; Roach et al. 2021; Williams et al. 2021), ocean acidification (Putnam et al. 2016; Sogin et al. 2016), coral/non-coral interactions (Quinn et al. 2016; Matthews et al. 2020; Roach et al. 2020), and chemical pollutants (Stien et al. 2019, 2020) on the coral metabolome. However, metabolomics analyses have not been used to investigate the molecular impacts and pathophysiology of coral diseases such as GAs.

The finger coral *Porites compressa* is an important reef-building coral in the Hawaiian Islands and is common to the reefs of Kaneohe Bay, Oahu (Bahr et al. 2015). The bay has been a site of high GA occurrence since the 1990s when they were first observed in *P. compressa* (Domart-Coulon et al. 2006; Stimson 2011). Despite research efforts to characterize the disease, the causative agents and specific biochemical impacts of GAs in *P. compressa* are still poorly understood. As a part of a larger endeavor to characterize GAs, *P. compressa* samples from Kaneohe Bay were previously characterized using morphological, elemental, and boron isotope analyses (Andersson et al. 2020). These efforts identified a novel GA lesion morph and demonstrated that the pH was lower in the internal calcifying fluid of GAs compared to healthy samples. Here, we expand on this previous work by using an untargeted  $^1\text{H}$  nuclear magnetic resonance (NMR) metabolomics approach to examine GAs from the same *P. compressa* samples in order to further elucidate the metabolic impacts these lesions have on affected colonies.

## Materials and methods

### Sample collection and processing

Coral samples were collected according to methods from Andersson et al. (2020), a conjoining study analyzing the elemental composition of skeletons from the same samples described here. In brief, samples (approximately 4 cm in diameter) were collected by hammer and stainless-steel chisel directly north of Coconut Island at depths less than 3 m within a 1 h period in March 2014 (State of Hawaii Division of Aquatic Resources Special Activity Permit 2011–1). Samples of three visually determined treatment groups were collected from individual diseased and healthy

*P. compressa* colonies: coral fragments exhibiting GAs (GA,  $n = 15$ ), apparently normal fragments directly adjacent to (i.e., touching) GA lesions on the same colony (unaffected,  $n = 15$ ), and apparently normal fragments from the nearest, distinct, adjacent colony free of GAs (approximately 0.05–2 m away; reference,  $n = 15$ ) (Fig. 1). Each GA sample was further categorized based on the morphology of the GA lesion as either a traditional, bulbous GA (Form 1) or a less protuberant, novel GA morph (Form 2) that was first described during our morphological characterization of these samples (Fig. 1b–c) (Andersson et al. 2020). In this way, a total of 45 samples were collected from 30 individual coral colonies. Samples were collected into Teflon bags and brought directly to the surface where the seawater was poured from the bags, and the bags were sealed with zip ties and frozen in liquid nitrogen ( $\text{LN}_2$ ) to preserve the physiological state of the samples.

Samples were generally processed following procedures recommended for metabolomics analysis of reef-building corals outlined by Andersson et al. (2019). Frozen samples were transferred from  $\text{LN}_2$  and freeze-dried in a VirTis Genesis OX lyophilizer with a Wizard 2.0 controller (SP Industries Inc., Warminster, USA). Subsequent sample handling time and exposure to air were limited to reduce contamination and partial rehydration of the soft tissues. In some cases, the GA lesion could not be cleanly separated from the surrounding tissues during sample collection underwater. In these cases, the GA and unaffected samples were therefore collected simultaneously as a single fragment (e.g., Fig. 1b) and the GA lesions were separated from surrounding unaffected coral by hammer and stainless-steel chisel after lyophilization. Firm-bristled plastic brushes were then used to collect the dry, soft tissue powders from the coral samples by evenly brushing the entirety of each fragment ( $\sim 10$  s per fragment area). These powders served as the primary materials for  $^1\text{H}$  NMR analysis and were comprised of various parts of the holobiont including the coral soft tissues, symbiotic dinoflagellates, associated microbial communities, and skeletal powder incidentally removed during brushing.

### Metabolite extraction for $^1\text{H}$ NMR metabolomics

Samples were extracted and analyzed using  $^1\text{H}$  NMR spectroscopy in four batches on consecutive days, with each batch containing three or four randomly selected sets (paired GA and unaffected samples from the same coral colony and corresponding reference sample from an adjacent colony) of *P. compressa* tissue powders. Each batch also consisted of a coral homogenate control material sample and blank sample to monitor for analytical

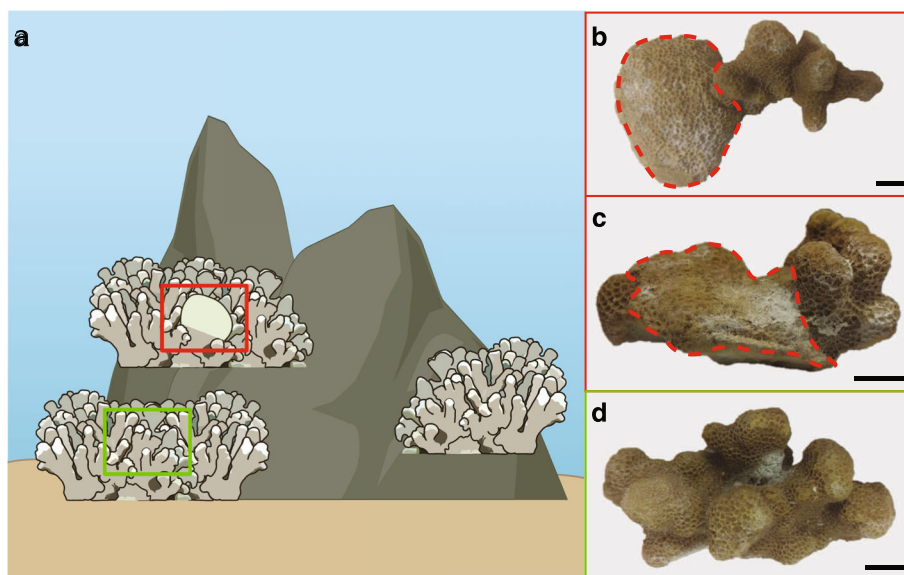


**Fig. 1** Overview of *Porites compressa* sampling strategy and different sample types that were collected. **a** Diagram depicting a *P. compressa* growth anomaly (GA) and unaffected sample pair collected from a GA-impacted colony (red box) and corresponding reference sample collected from the nearest, distinct, adjacent *P. compressa* colony (green box). Representative photographs of **b** Form

1 GA lesion and paired unaffected sample, **c** Form 2 GA lesion and paired unaffected sample, and **d** reference coral sample taken in the laboratory after lyophilization. (**b–d**) Dashed red outlines indicate GA lesions, and unmarked areas show apparently normal (unaffected or reference) coral; black bars indicate 1 cm

reproducibility across batches and possible method contaminants, respectively.

Metabolites were extracted from the tissue powders (all samples were standardized to  $100 \text{ mg} \pm 3 \text{ mg}$  prior to extraction) using methods modified from Bligh and Dyer (1959) and Wu et al. (2008), as recommended for reef-building corals by Andersson et al. (2019). In short, a biphasic solvent system consisting of chloroform, methanol, and water at a final ratio of 2:2:1.8 was used to extract metabolites from the tissue powders (see Supplemental Text for full details). The polar metabolite-containing fraction of each extract was transferred using a glass pipette into a microcentrifuge tube and dried in a Vacufuge Concentrator 5301 (Eppendorf AG, Hamburg Germany) at room temperature. The mass of the dried metabolite pellet from each sample was recorded as the extract mass.

After extraction, the residual material was then placed in bleach (5.65–6% Laboratory Grade Sodium Hypochlorite Solution) and rotated using a Roto-Shake Genie SI-1100 (SP Scientific Inc., New York, USA) for 24 h to oxidize and solubilize all remaining organics. After bleach was removed, the remaining calcium carbonate powder was then rinsed with water, dried, and weighed to record the mass of non-target skeleton that contributed to the tissue powder extraction mass. The total amount of tissue extracted from each sample was then estimated by subtracting the weight of skeletal contamination from the initial weight of the tissue powder. The extract yield (extract mass by total mass of tissue extracted) was also

calculated for each sample as a normalized estimate of the extract mass.

### NMR spectroscopy data collection and processing

Dried metabolites were rehydrated in  $600 \mu\text{L}$  of deuterium oxide-based 0.1 M sodium phosphate buffer containing 1 mM of 3-trimethylsilylpropionic-2,2,3,3,-d, acid sodium salt (TMSP) as a NMR chemical shift reference peak. Samples ( $550 \mu\text{L}$ ) were then transferred to 5-mm NMR tubes (NORELL, Inc., Morganton, North Carolina, USA) for  $^1\text{H}$  NMR analysis. All NMR profiles were obtained using a 700 MHz Bruker NMR spectrometer equipped with a TCI cryoprobe and a SampleJet autosampler. One-dimensional (1D)  $^1\text{H}$  NMR spectra were acquired (Topspin version 3.2) using a nuclear Overhauser effect spectroscopy pulse sequence consisting of 8 dummy scans and 256 scans for 65,536 data points with a relaxation delay of 3 s. Spectra were produced from the acquired free induction decay (FID) via Fourier transformation. Spectra were referenced, phased, and baseline-corrected automatically (Topspin version 3.2).

Two-dimensional (2D) NMR spectra were acquired using a  $^1\text{H}$ – $^{13}\text{C}$  heteronuclear single quantum correlation (HSQC) experiment to resolve the spectral overlap in the 1D spectrum (Ross et al. 2007; Markley et al. 2017) and confirm structural identification. The HSQC data were acquired with 128 scans from 2048 data points from the 512 increments in the F1 dimension. Sweep widths of

10.98 ppm (F2) and 180.0 ppm (F1) were used. A relaxation delay of 1.5 s between acquisitions was used along with a refocusing delay of 30 ms. The FIDs were weighted using a shifted sine bell function in both dimensions, and chemical shifts were referenced to the internal TMSF signal.

### Reproducibility and quality control

Analytical and methodological reproducibility across batches were assessed by evaluation of inter-batch control material samples. An in-house *Orbicella faveolata* control material was used for these samples to conserve the limited quantities of the experimental coral tissue powders. A full description of the *O. faveolata* control material and the reproducibility of control material and experimental spectra can be found in supplementary materials (Supplemental Text; Fig. S1; Fig. S2). Samples utilized for method optimization (sample identifications: ‘unaffected-14’ and ‘GA-14’) (Andersson et al. 2019) were excluded from all statistical analyses. Samples where methodological error prevented the measurement of the extract mass (sample identifications: ‘unaffected-1’ and ‘GA-2’) or the mass of tissue extracted (sample identifications: ‘unaffected-4,’ ‘reference-7,’ ‘reference-9,’ ‘reference-11,’ and ‘reference-14’) were also excluded from all statistical analyses and analyses of extract data, respectively (Table S1).

### Statistical analyses

Metrics of metabolite extraction were compared between GA, unaffected, and reference samples using univariate analyses. Parametric one-way analysis of variance (ANOVA) models with Tukey honestly significant difference (HSD) post hoc tests were conducted to compare the mass of total tissue extracted, extract mass, and extract yield.

To facilitate statistical analysis of the  $^1\text{H}$  NMR metabolomics data, peaks were aligned using the least square method with a max shift of 0.05 ppm to correct for small variations in chemical shift across samples using NMRProcFlow v1.2 (Jacob et al. 2017). An adaptive, intelligent binning procedure was subsequently performed on the spectra from 0.2 to 10 ppm with a signal-to-noise threshold equal to 3:1 (De Meyer et al. 2008). This procedure assigned spectral features (peaks) into bins, thereby excluding spectral noise (non-peaks) from downstream analyses. Residual water (4.7–5.0 ppm) and other contaminants detected in the blank sample spectra (Table S2; Fig. S3) were precluded from binning, and bins that contained only noise were removed manually. Remaining bins (330 total) were exported as data tables and normalized by extract mass (Fig. S4) to enable relative comparisons of

metabolomic profiles. For annotated features that spanned multiple bins (i.e., two bins containing separate peaks of a putative doublet), statistical results were presented from a selected representative bin.

Multivariate analyses were conducted using Metaboanalyst 4.0 (Xia and Wishart 2016) where bins were mean-centered and Pareto-scaled in order to decrease the dominance of bins with the largest intensities (van den Berg et al. 2006) prior to principal component analysis (PCA). PCAs were used to visually assess the quality of the data and to evaluate trends within and among treatment groups. Partial least squares discriminant analysis (PLS-DA) models were used as a supervised multivariate approach to help determine bins that differed between treatment groups that displayed divergence in PCA.

Predictive ability of PLS-DA models ( $Q^2$ ) was evaluated with a tenfold cross-validation of the first two components, and model quality was further assessed with permutation tests by group separation distance with 1000 permutations (Bijlsma et al. 2006; Syzmanska et al. 2012). Twenty sub-models were created for each PLS-DA model to evaluate reproducibility of validation metrics, and the averages were reported as iterative  $Q^2$  (cross-validation) and  $p$ -values (permutation tests). Variable importance in projection (VIP) scores were used to rank important bins and were calculated for each bin by averaging the scores of the first two components.

Each set of unaffected and GA samples were collected from the same coral colony; therefore, additional multivariate analyses were used in order to increase resolution by focusing on unaffected–GA pairs to discount inter-colony variation. An average metabolic change vector (AMCV) was calculated from a PCA of intact unaffected–GA pairs by averaging of the difference in PCA scores between each unaffected–GA pair. The AMCV was multiplied by the PCA loadings of each bin to give a modified loadings score indicating its contribution toward the AMCV (Southam et al. 2008). The bins that provided the largest contributions to the AMCV were determined as the inflection point of the plotted cumulative sum of the AMCV loadings (Fig. S5).

Univariate analyses were subsequently used to further elucidate patterns from multivariate approaches. Parametric one-way ANOVA models were used to compare relative intensities in  $^1\text{H}$  NMR spectra (normalized by extract mass) for all bins between all three treatments. Additionally, paired  $t$  tests were conducted to compare all bin intensities between intact pairs of GA and unaffected samples ( $n = 24$ ). Corrections to account for multiple statistical tests were used to separately adjust the  $p$ -values from the ANOVA and paired  $t$  tests of the spectral bins, using the false discovery rate method (Benjamini and Hochberg 1995) for both corrections. Distribution

normality and homoscedasticity of variables for all univariate analyses were evaluated graphically.

### Metabolite identification

A full spectrum annotation was conducted using a representative 1D  $^1\text{H}$  NMR spectrum and 2D  $^1\text{H}$ - $^{13}\text{C}$  HSQC spectrum from each of the three treatment groups in order to identify as many metabolites as possible in the *P. compressa* extracts. Metabolites were annotated using Chenomx NMR Suite (v8.31; Edmonton, Alberta, Canada) 700 MHz spectral libraries to match peak shape and intensity from the 1D  $^1\text{H}$  NMR spectra. Additionally, 2D  $^1\text{H}$ - $^{13}\text{C}$  HSQC data were used to match resonances from the Human Metabolome Database (Wishart et al. 2007) and the Biological Magnetic Resonance Bank (Ulrich et al. 2008) metabolite databases to complement putative metabolite identifications from 1D annotations. Spectral features that could not be assigned a metabolite identification were annotated as unknowns. Splitting pattern,  $^1\text{H}$ , and  $^{13}\text{C}$  chemical shifts were also recorded for identified and unknown spectral features. Annotated features were matched to the spectral bins used for statistical analyses to facilitate biological interpretations.

## Results and discussion

### Metabolome annotations

The full spectrum annotation resulted in the identification of 18 (8.1% of total annotated features) putative metabolites, 12 (5.6% of total annotated features) of which were supported by 2D HSQC resonance chemical shifts (Table 1; Fig. S6), in addition to 204 unknown spectral features (Table S3). All putatively identified metabolites were present in all three treatment groups. Previous annotations of *P. compressa* metabolomes resulted in only two putatively identified compounds (Sogin et al. 2014), both of which (alanine, glucose) were also found in our spectra. In both cases, glucose was present in low concentrations compared to other features in the metabolomic profile of *P. compressa* (Fig. S6) (Sogin et al. 2014). Glucose is an energetically and physiologically important coral metabolite (Burriesci et al. 2012; Ochsenkuhn et al. 2017; Hadaidi et al. 2019) that is commonly identified in metabolomic profiles of other coral species (e.g., Putnam et al. 2016; Sogin et al. 2016; Hillyer et al. 2017). In contrast to *P. compressa*, glucose is one of the most abundant metabolites measured in other coral species such as *Acropora aspera* (Hillyer et al. 2017). Furthermore, known coral-associated metabolites such as trehalose (Hagedorn et al. 2015), floridoside (Ochsenkuhn et al.

2017), and arabinose (Hadaidi et al. 2019) were not visible in our *P. compressa* spectra at all. Reasons for such species-specific differences in these metabolites are unclear but will be of interest going forward.

Previous NMR-based coral identifications have typically relied on matching 1D  $^1\text{H}$  shifts to metabolite databases, resulting in level 2 (putative) identifications as classified by the Metabolomics Standards Initiative (Sumner et al. 2007). Level 2 identifications are generally susceptible to misidentification because they do not utilize authentic chemical standards, and identification of coral metabolites is further limited by the scarcity of metabolite database resources devoted to non-model organisms. Therefore, to increase annotation rigor, we annotated as many features as possible from the entire spectrum while implementing complementary 2D  $^1\text{H}$ - $^{13}\text{C}$  HSQC data, in addition to 1D  $^1\text{H}$  spectra.

Although still producing level 2 identifications, this approach increased the confidence of metabolite identity by providing crucial information regarding atom connectivity. The 18 (8.1% of total annotated features) putative metabolites we identified are comparable in number to other NMR-based coral metabolomics studies (e.g., 3–26 identifications (11.1–28.6% of total annotated features, 1D only)) (Sogin et al. 2014; Putnam et al. 2016; Lohr et al. 2019b). NMR-based studies typically seem to report fewer putative metabolite identifications compared to their mass spectrometry-based counterparts, which generate high feature numbers despite similar putative identification capacity for both analytical methodologies (e.g., 99–271 identifications (11.2–22.3% of total annotated features)) (Sogin et al. 2016; Hillyer et al. 2017; Lohr et al. 2019b). Annotation results are also influenced by differences in the number and type of coral species analyzed, ionization and detection strategy of the measurement tool, and metabolite identification rigor. In comparison, 204 features from our spectra were annotated as unknowns, including many of the features with the highest relative intensities (e.g., Unknowns #72, 73, 58, 82, 68, 71) (Table S3; Table S4), further demonstrating the need for improved metabolite databases for non-model organisms such as coral.

While all levels of metabolite identification can be useful for preliminary probes of coral metabolism, increased identification confidence is necessary to establish foundational knowledge of coral metabolomes and to generate high-quality metabolic pathway hypotheses to be tested. Therefore, our more rigorously annotated putative metabolites provide increased confidence to the metabolic pathway analyses discussed in the following sections. Furthermore, our annotation efforts bolster the amount of high-quality metabolite data available in this developing field, which can be used as a reference to aid annotation efforts in future studies. This will help the field transition

**Table 1** Putatively identified metabolites from representative growth anomaly, unaffected, and reference *Porites compressa* spectra

Compound	<sup>1</sup> H Shifts (ppm)	<sup>13</sup> C Shifts (ppm)	HMDB Identifier	Fig. S6 Label
1-Methylnicotinamide	<b>9.27 (s), 9.00 (d), 8.89 (d), 8.17 (t), 4.47 (s)</b>	<b>147.8, 150.0, 146.3, 130.8, 51.3</b>	HMDB-0000669	1
2'-Deoxyadenosine	<b>8.30 (s), 8.20 (s)</b> , 6.45, 4.64, 4.18, 3.83, 3.79, 2.82, 2.56	143.1, 155.2, 87.4, 74.1, 90.2, 64.4, 64.4, 41.8, 41.8	HMDB-0000101	2
Alanine	3.76, <b>1.49 (d)</b>	53.6, 19.0	HMDB-0000161	3
Betaine	<b>3.89 (s), 3.25 (s)</b>	<b>68.6, 55.9</b>	HMDB-0000043	4
Carnitine	<b>4.56 (m)</b> , 3.42, <b>3.22 (s), 2.43 (m)</b>	<b>66.7, 72.7</b> , 56.8, <b>45.6</b>	HMDB-0000062	5
Glucose	<b>5.22 (d), 4.63 (d)</b> , 3.90, 3.83, 3.82, 3.74, 3.70, 3.52, 3.47, 3.39, 3.24	94.9, 98.7, 63.5, 63.4, 74.1, 63.4, 75.6, 74.2, 78.6, 72.3, 77.0	HMDB-0000122	6
Glucose-1-phosphate	<b>5.44 (m)</b> , 3.91, 3.77, 3.47, 3.38, 3.86	<b>96.5</b> , 74.8, 75.9, 75.1, 72.5, 63.5	HMDB-0001586	7
Glycine	<b>3.55 (s)</b>	<b>44.3</b>	HMDB-0000123	8
Histamine	<b>7.92 (s), 7.12 (s)</b> , 3.29, 3.01	<b>138.7, 119.1</b> , 41.9, <b>26.9</b>	HMDB-0000870	9
Isoleucine	3.65, 1.96, 1.45, <b>1.00 (d)</b> , 0.93	62.5, 38.7, 27.0, 17.4, 13.9	HMDB-0000172	10
Isopropanol	4.01, <b>1.16 (d)</b>	67.1, 26.4	HMDB-0000863	11
Leucine	3.74, 1.70, 1.71, <b>0.96 (d), 0.94 (d)</b>	56.2, 42.6, 26.8, <b>24.8</b> , 23.6	HMDB-0000687	12
Lysine	3.75, 3.02, 1.88, <b>1.72 (m)</b> , 1.49, 1.43	57.5, <b>42.1, 32.7, 29.2</b> , 24.0, 24.0	HMDB-0000182	13
Methanol	<b>3.37 (s)</b>	<b>51.4</b>	HMDB-0001875	14
Methylamine	<b>2.59 (s)</b>	<b>27.6</b>	HMDB-0000164	15
Trigonelline	<b>9.17 (s)</b> , 9.07, <b>8.88 (d)</b> , 8.80, <b>8.08 (t), 8.88 (d)</b> , 8.78, <b>4.44 (s)</b>	<b>148.4</b> , 148.4, <b>147.5</b> , 147.6, <b>130.4, 148.7</b> , 148.7, <b>51.1</b>	HMDB-0000875	16
Tyrosine	<b>7.19 (d), 6.89 (d)</b> , 3.93, 3.17, 3.07	<b>133.5, 118.9</b> , 59.0, 38.3, 38.3	HMDB-0000158	17
Valine	3.60, 2.26, <b>1.03 (d), 0.98 (d)</b>	63.3, 31.9, 20.8, 19.4	HMDB-0000883	18

Bolded chemical shifts were matched in the <sup>1</sup>H or heteronuclear single quantum correlation (HSQC) nuclear magnetic resonance (NMR) spectra; unbolded chemical shifts were not matched due to overlap or detection limits. Listed NMR chemical shift values correspond to human metabolome database (HMDB) reference spectra. Splitting pattern of matched shifts on <sup>1</sup>H NMR spectra is indicated in parentheses; symbol 's' indicates singlet, 'd' indicates doublet, 't' indicates triplet, and 'm' indicates multiplet

from utility-based to more experimental studies, with critical biological interpretations and future research directions (e.g., targeted studies) depending largely on such identifications.

### GA impacts on coral metabolism

We used two approaches to assess differences in metabolism between *P. compressa* samples. (1) The extract yield was used to evaluate the overall metabolic output of the samples. Additionally, (2) the composition and relative abundance of measured metabolites (i.e., metabolomic profiles) in GA, unaffected, and reference samples were used to assess GA impacts on coral metabolism and specific metabolic pathways. The use of the extract data provided complementary metabolic information regarding the absolute metabolism of these samples that would be overlooked if only the relative comparisons of normalized

metabolomic profiles were to be considered. It should be noted that these masses consist of the entire suite of metabolites (and potentially other process carryover contaminant molecules) contained in the extract polar fraction. Therefore, while differences may provide a general overview of metabolic activity, discerning the effects of specific metabolites or metabolite classes is not possible using this method alone. Furthermore, this method is confounded by any inherent differences in extraction efficiency between GA and healthy tissues.

The extract yield was nearly identical for unaffected and GA samples (Tukey HSD post hoc  $p = 0.983$ ); however, for reference samples it was approximately 66% and 70% that of unaffected and GA samples, respectively (ANOVA  $F_{2,33} = 5.106$ ,  $p = 0.012$ ) (Fig. 2a; Table S5). In order to sustain their elevated skeletal and tissue growth (Domart-Coulon et al. 2006), GAs rely on nutrient imports from surrounding unaffected tissues (Stimson 2011) as well as

local resources re-allocated from other vital biological functions such as reproduction, energy storage in the form of lipids, and internal pH regulation (Domart-Coulon et al. 2006; Palmer and Baird 2018; Sale et al. 2019; Andersson et al. 2020). Our results seemingly indicate an increase in overall metabolic activity in both GA lesions and apparently healthy (unaffected) areas from GA-impacted colonies compared to GA-free colonies. This increased metabolic activity in GAs may be linked to the energy burden the lesions impose on affected colonies and further demonstrates that the metabolic impacts of GAs are not limited to the lesions themselves.

Metabolomic profile differences were evaluated through PCA of all samples, which showed large amounts of overlap between GA, unaffected, and reference treatments, with particularly high overlap between unaffected and reference samples. Therefore, PCA scores alone were not useful for distinguishing to which treatment group a given sample belongs (Fig. 2b). Isolated comparisons across treatments (GA–unaffected, unaffected–reference, GA–reference) again showed high similarity of samples in PCA (Fig. S7a–c), indicating the extent of GA impacts on metabolomic profiles is low compared to other sources of variation, such as differences between individual coral colonies. These results contrast with the clear morphological, histological, and physiological differences previously documented in *P. compressa* GAs (Domart-Coulon et al. 2006). Furthermore, other stressors such as temperature and coral-neighbor interactions generally do result in group separation of coral metabolomes in PCA or principal coordinates analysis plots (Quinn et al. 2016; Hillyer et al. 2017).

PCA of only GA and reference samples showed group separation along the second principal component (PC 2; 25.6% explained variance (EV)) (Fig. S7c) and comparison of these two sample types therefore warranted further investigation using supervised PLS-DA. Validation of the PLS-DA model comparing GA to reference samples (Fig. S7d) indicated an effect of treatment ( $p = 0.034 \pm 0.001$ ; mean  $\pm$  SE), but the predictive power ( $Q^2 = 0.394 \pm 0.013$ ; mean  $\pm$  SE) of the model was low (Szymanska et al. 2012). Therefore, a conservative VIP threshold (VIP > 2) (i.e., Lohr et al. 2019b) was used to identify 13 important features from the model, all of which were annotated as unknowns (Table S6).

PCA plots were also used to assess differences in metabolomic profiles between bulbous Form 1 GAs and the less protuberant Form 2 GAs. Form 1 samples generally had less metabolic variation and appeared to be slightly different compared to Form 2 samples in PC 2 (22.0% EV) (Fig. S8). However, small sample size and imbalanced replication of Form 1 ( $n = 9$ ) and Form 2 ( $n = 3$ ) lesions precluded the use of meaningful univariate or supervised multivariate analyses here. Therefore, despite consistent macro-morphological differences and preliminary evidence for trace elemental and metabolomic differences (Andersson et al. 2020), more research is necessary to confirm these two morphs as distinct *P. compressa* GA lesions.

Subsequent univariate comparisons across GA, unaffected, and reference samples showed average spectral intensities between groups were similar for nearly all features and did not highlight any new features of interest. However, Unknown #86 at 3.37 ppm did have higher intensities in both unaffected and reference compared to GA samples (ANOVA  $F_{2,38} = 13.321$ ,  $p = 0.014$ )

**Fig. 2 a** Average extract yield for growth anomaly (GA;  $n = 13$ ), unaffected ( $n = 12$ ), and reference samples ( $n = 11$ ). Points indicate group mean, and error bars indicate standard error of the mean. Displayed  $p$ -value is from one-way analysis of variance model;  $p$ -values for specific post hoc comparisons are listed in Table S5. **b** Principal component analysis scores plot of the first two principal components (PC 1 and PC 2) for GA ( $n = 13$ ), unaffected ( $n = 13$ ), and reference samples ( $n = 15$ ). Ellipses indicate 95% confidence region of the multivariate t-distribution for each group

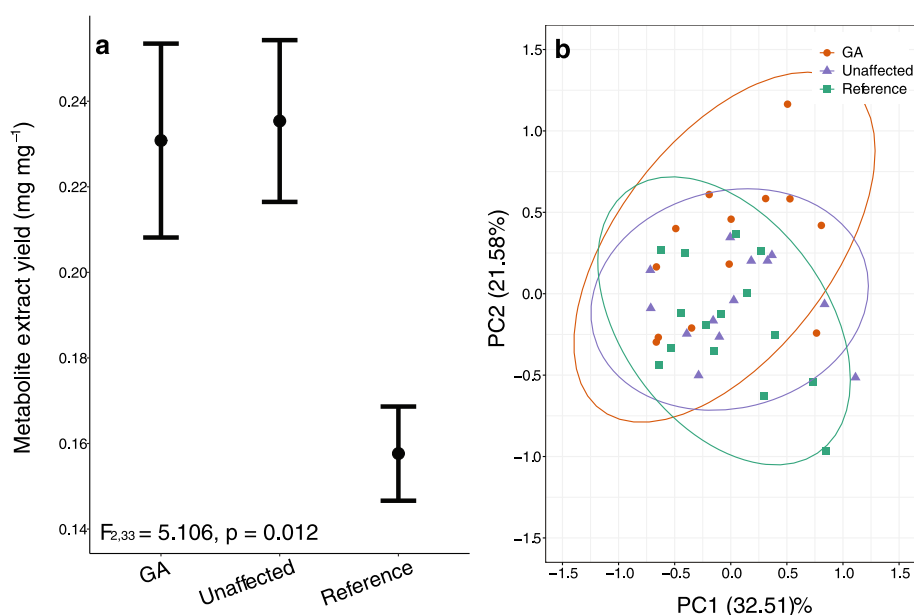


(Table S4), supporting the importance of this feature in the PLS-DA model (VIP = 2.34) (Table S6). Full statistical results for all 330 bins are presented in Table S4. Collectively, these results showed that any detectable, systematic differences GAs imposed on coral metabolomes were largely confounded by relatively high inter-colony variation among the samples.

Individual coral species generally have distinct and relatively consistent metabolomic profiles (Sogin et al. 2014; Putnam et al. 2016; Andersson et al. 2019), yet variation among individuals of the same species is sufficient to allow for the distinction of unique genotypes using PCA (Lohr et al. 2019b). As we have demonstrated above, this variation can obscure systematic differences in the presenting phenotypes. A similar phenomenon was observed during our previous elemental characterization of these samples, where differences in certain trace elements (e.g., Mg/Ca, U/Ca, Va/Ca, Mo/Ca) and internal pH were only apparent once paired analyses of unaffected and GA samples were implemented (Andersson et al. 2020). Therefore, we continued our characterization of GA metabolomic profiles below by capitalizing on the unique paired status of the GA and unaffected samples collected from the same colony (genotype), which allowed for more explicit investigation of disease-related metabolic shifts by controlling for inter-colony variation.

### Analysis of paired metabolomic profiles

Visual inspection of the PCA for only paired GA and unaffected samples (combined 57.2% EV for PC 1 and PC 2) again showed considerable group overlap (Fig. 3). However, a consistent pattern can be observed between each paired set of samples, with all unaffected samples (except sample 7U) having a lower PC 2 (20.9% EV) score than their respective GA sample. This indicated a consistent metabolic shift between unaffected and GA samples, which was obscured by the relatively larger inter-colony variation. The observed variation between individual unaffected–GA pairs could be due to a variety of genetic, environmental, or disease-progression factors. Therefore, collecting additional genetic data (e.g., DNA or RNA) or controlling environmental variables (e.g., diet, neighbor interactions) may help interpret this variability in future GA studies.

An AMCV was calculated to determine which features were primarily responsible for driving the constant shift between paired samples in the PCA scores plot (Fig. 3). Modified loadings scores were created to determine the contribution of each feature toward the AMCV (Fig. S9), and the 41 features with largest contribution to the AMCV (see Fig. S5) are highlighted in Table 2, while loadings for all features are listed in Table S4. Paired *t* tests separately

identified a total of 61 features that differed between unaffected and GA samples (paired *t* test  $p < 0.05$ ) (Table S4). Of the 41 most influential AMCV features, 29 differed according to univariate analyses as well ( $p < 0.05$ ) (Table 2). A combined total of 73 unique features were identified by either multivariate or univariate analyses, and these trends were confirmed visually using the raw data (e.g., Fig. 4; Fig. S10; Table S4). These results highlight the benefits of collecting and analyzing paired samples in coral metabolomics research when possible, where inherent metabolome variation between individual coral colonies can be a challenge.

Of these features, 1-methylnicotinamide, trigonelline (GA high), betaine, glycine, and histamine (GA low) were putatively identified (Table 2). Betaine and glycine were influential in the AMCV, while univariate analyses provided evidence of differences between GA and unaffected samples for betaine ( $t_{11} = -2.685$ ,  $p = 0.060$ ), glycine ( $t_{11} = -3.403$ ,  $p = 0.032$ ), histamine ( $t_{11} = -2.966$ ,  $p = 0.046$ ), trigonelline ( $t_{11} = 3.077$ ,  $p = 0.041$ ), and 1-methylnicotinamide at 8.86 ppm ( $t_{11} = 3.342$ ,  $p = 0.032$ ) and 8.95 ppm ( $t_{11} = 3.203$ ,  $p = 0.036$ ) (Table 2). It should be noted that glycine and Unknown #102 overlapped in the same statistical bin, although both features appeared to be low in GA compared to unaffected samples by direct spectral comparison (Fig. S10).

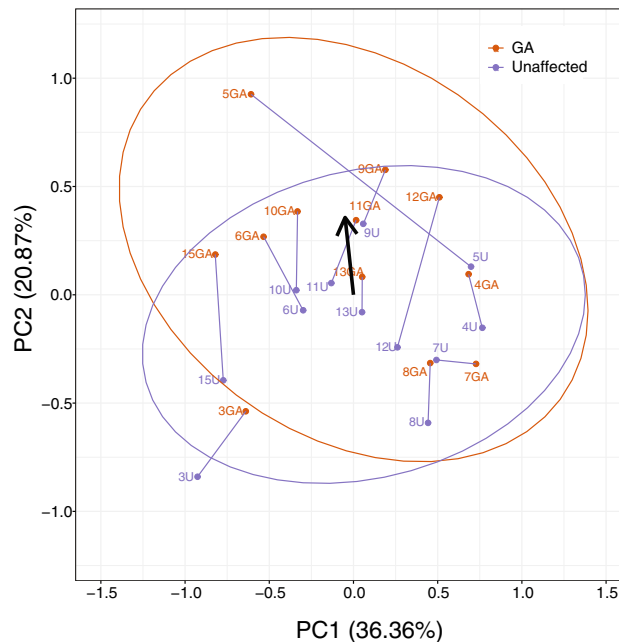


**Fig. 3** Principal component analysis (PCA) scores plot of the first two principal components (PC 1 and PC 2) for paired growth anomaly (GA;  $n = 12$ ) and unaffected samples ( $n = 12$ ). Blue lines indicate the difference in PCA scores between each unaffected–GA pair, and the bold arrow indicates the average metabolic change vector from unaffected to GA samples. Ellipses indicate 95% confidence region of the multivariate *t*-distribution for each group

Many of the most influential features identified by both the unpaired (Table S6) and paired (Table 2) analyses were annotated as unknowns, restricting pathway analyses to only a handful of compounds (see Supplemental Text for in-depth comparison of unpaired and paired results). These unknown features are of interest regarding GA pathophysiology, and more effort is therefore needed to identify important unknown compounds through isolation and spectroscopic techniques. Nonetheless, using known biochemical activities of identified compounds can provide a useful starting point for generating testable hypotheses regarding specific metabolite activity or metabolic pathways that may be associated with GA pathophysiology in *P. compressa*. Although differences in the five putative metabolites were difficult to detect without the advantage of paired unaffected and GA samples, even subtle changes in tightly regulated metabolites may be physiologically important. Therefore, the features contributing to this shift are good candidates for providing insights into the molecular pathology of GAs, and preliminary pathway analyses of putatively identified metabolites are discussed below.

### Metabolic pathway analyses

Betaine is an important organic osmolyte (Ashraf and Foolad 2007) and has been shown to accumulate in marine invertebrates in response to environmental stress (Liu et al. 2011; Cappello et al. 2013), including other reef-building coral species (Williams et al. 2021). However, we observed low betaine levels in GA samples despite their abnormal condition that could be expected to trigger such an accumulative stress response. Alternatively, this may be explained by betaine accumulating in the unaffected tissues as a stress response to the directly adjacent GA lesions, or by a decreased influx of symbiont-derived betaine in GAs due to their lower abundance of symbiotic dinoflagellates (Domart-Coulon et al. 2006).

Glycine is an amino acid precursor (Amelio et al. 2014) that is highly abundant in the skeletal organic matrix secreted by corals (Puverel et al. 2005). The organic matrix is thought to act as a biological framework during skeleton formation, and the glycine composition of this matrix differs between corals with distinct skeleton morphologies (Puverel et al. 2005). This indicates that the amino acid composition of the organic matrix may affect skeleton structure and/or morphology, and thus, the decreased levels of glycine we measure in GAs may be linked to their irregular skeletal characteristics. Our previous elemental work on these samples indicates that GAs allocate resources away from the pH regulation of their calcifying fluid to sustain their rapid growth (Andersson et al. 2020). If this is the case, GAs may also allocate energy away from

other aspects of skeletogenesis, such as glycine synthesis for the organic matrix. Alternatively, it may be that the faster extending skeletons of *P. compressa* GAs (Domart-Coulon et al. 2006) are depleting glycine levels, thereby contributing to the low glycine we measure in GA compared to unaffected samples.

Betaine and glycine together belong to a larger set of biochemical pathways involved in glycine/serine metabolism, specifically the oxidation of choline to glycine, which can then be interconverted with serine (Fig. 5). The decreased levels of betaine and glycine indicate a down-regulation in the choline oxidation pathway in GAs. In the cnidarian model *Aiptasia*, choline-derived synthesis of glycine is upregulated in non-symbiotic individuals, a proposed indicator of heterotrophic feeding (Cui et al. 2019). The lower choline oxidation we theorize in GA samples would then indicate a decrease in choline-derived glycine (Fig. 5) and thus a decreased proportion of heterotrophic feeding in GA lesions.

GAs in *P. compressa* contain fewer symbiotic dinoflagellates compared to unaffected tissues (Domart-Coulon et al. 2006), so it might be expected that these lesions increase heterotrophic feeding to compensate for the assumed decreased influx of photosynthates. However, unlike some coral species, *P. compressa* does not increase heterotrophic feeding to compensate for the loss of symbionts during bleaching (Grottoli et al. 2006), which may explain why feeding is seemingly not increased in GAs. Additionally, the abnormal polyp characteristics of GAs may restrict their ability to capture prey. For example, *P. compressa* GAs have fewer and more dispersed polyps (Domart-Coulon et al. 2006; Andersson et al. 2020), which may reduce heterotrophic feeding potential. If true, an inability for heterotrophic feeding to compensate for the loss of symbiont-derived resources in GA lesions may contribute to the energetic burden that GA tissues place on the rest of the coral holobiont to sustain their growth. Increased skeletal Mo/Ca and V/Ca in these same GA samples may indicate decreased nitrogen fixation in the GA holobiont as well (Andersson et al. 2020), which would only exacerbate GA reliance on external energy sources.

The choline oxidation pathway is also linked to DNA methylation through the 1-carbon cycle (Fig. 5). DNA methylation often functions to inhibit expression of unwanted genes (Niculescu and Zeisel 2002) and is a known mechanism for phenotypic plasticity in corals as an acclimatization response to environmental stress (Putnam et al. 2016). Moreover, metabolomics analysis of benign hepatic tumors in flatfish revealed decreases in both choline and glycine (Southam et al. 2008), and choline-deficient diets can induce hepatocellular carcinomas in rats (Nakae et al. 1992). Although these results do not necessarily support the classification of GAs as tumors (malignant or

**Table 2** Top 41 features contributing to the average metabolic change vector (AMCV) between paired growth anomaly (GA) and unaffected samples, along with false discovery rate corrected p-values from paired t tests given in order of increasing <sup>1</sup>H nuclear magnetic resonance (NMR) chemical shift

<sup>1</sup> H shift (ppm)	<sup>13</sup> C shift (ppm)	Annotation	Splitting	p-value (t-value; df)	Trend	AMCV loading
1.57	15.4	Unknown #7	m	0.903 (0.164;11)	GA low	-1.989
1.61	23.4	Unknown #8	m	0.021 (4.147;11)	GA high	2.595
1.87	22.7	Unknown #10	m	0.030 (3.595;11)	GA high	3.225
1.96	22.6	Unknown #12	d	0.038 (3.159;11)	GA high	2.934
1.97	No HSQC	Unknown #13	d	0.043 (3.021;11)	GA high	2.450
1.98	27.1	Unknown #14	d	0.036 (3.206;11)	GA high	3.318
2	No HSQC	Unknown #15	d	0.032 (3.386;11)	GA high	2.125
2.01	27.1	Unknown #16	d	0.046 (2.960;11)	GA high	3.119
2.12	27.1	Unknown #20	m	0.203 (1.685;11)	GA high	4.485
2.18	21.5	Unknown #22	m	0.042 (-3.044;11)	GA low	-3.878
2.29	28.1	Unknown #26	m	0.020 (-4.195;11)	GA low	-2.907
2.33	38.7	Unknown #29	t	0.024 (-3.780;11)	GA low	-2.436
2.37	38.8	Unknown #32	d	0.015 (-4.622;11)	GA low	-2.333
2.4	38.8	Unknown #33	d	0.012 (-4.947;11)	GA low	-2.242
2.51	28.1	Unknown #38	m	0.031 (-3.493;11)	GA low	-4.617
2.94	45.9	Unknown #58	s	0.032 (-3.467;11)	GA low	-2.203
3.13	51.5	Unknown #70	s	0.012 (-5.354;11)	GA low	-6.138
3.24	55.4	Unknown #75	s	0.040 (3.102;11)	GA high	6.904
3.26	47.6	Unknown #76	s	0.031 (3.498;11)	GA high	11.165
3.27	56.2	Betaine	s	0.060 (-2.685;11)	GA low	-2.874
3.28	50.4	Unknown #77	s	0.521 (-0.853;11)	GA low	-5.559
3.28	57.8	Unknown #78	s	0.521 (-0.853;11)	GA low	-5.559
3.29	55.6	Unknown #79	s	0.335 (1.246;11)	GA high	4.985
3.39	56.7	Unknown #87	s	0.167 (1.840;11)	GA high	2.870
3.41	50.7	Unknown #88	s	0.656 (0.613;11)	GA high	3.929
3.41	57.3	Unknown #89	s	0.031 (-3.542;11)	GA low	-7.119
3.48	47.3	Unknown #96	m	0.033 (3.320;11)	GA high	5.746
3.54	70.0	Unknown #101	m	0.075 (-2.478;11)	GA low	-5.238
3.56	70.1	Unknown #102	s	0.032 (-3.403;11)	GA low	-5.792
3.56	44.2	Glycine	s	0.032 (-3.403;11)	GA low	-5.792
3.58	70.1	Unknown #104	d	0.365 (-1.167;11)	GA low	-2.260
3.61	48.1	Unknown #106	m	0.037 (3.179;11)	GA high	2.693
3.62	67.9	Unknown #107	s	0.023 (3.948;11)	GA high	2.726
3.63	61.8	Unknown #110	s	0.046 (2.937;11)	GA high	2.268
3.72	70.1	Unknown #119	m	0.037 (-3.183;11)	GA low	-2.156
3.74	64.4	Unknown #121	m	0.040 (3.099;11)	GA high	6.037
4.03	49.4	Unknown #148	d	0.060 (2.668;11)	GA high	2.053
4.06	76.9	Unknown #150	s	0.024 (-3.790;11)	GA low	-2.116
4.08	79.3	Unknown #151	m	0.012 (-5.166;11)	GA low	-5.251
4.14	78.9	Unknown #155	m	0.055 (-2.777;11)	GA low	-2.505
4.39	79.2	Unknown #170	m	0.012 (-4.962;11)	GA low	-2.157
4.44	51.0	Trigonelline	s	0.041 (3.077;11)	GA high	1.094
7.13	119.2	Histamine	s	0.046 (-2.966;11)	GA low	-0.055
8.86	145.3	l-methylnicotinamide	s	0.032 (3.342;11)	GA high	0.401
8.95	149.8	l-methylnicotinamide	d	0.036 (3.203;11)	GA high	0.332

Any annotated features with p-values below 0.05 are also listed below, regardless of AMCV contribution. Positive and negative loading scores indicate features high and low in GA compared to unaffected samples, respectively. 'No HSQC' no detectable heteronuclear single quantum correlation resonance, 'df' degrees of freedom. Splitting pattern of shifts on <sup>1</sup>H NMR spectra is denoted as follows: 's' singlet, 'd' doublet, 't' triplet, 'm' multiplet

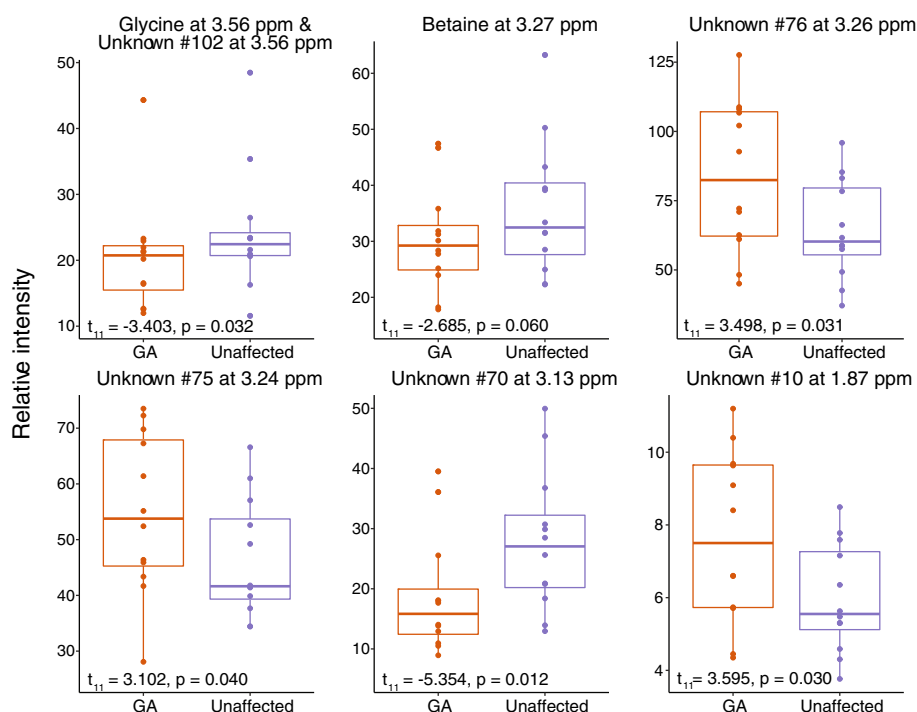


**Fig. 4** Boxplots showing relative intensity of growth anomaly (GA;  $n = 12$ ) and unaffected ( $n = 12$ ) samples of selected features of interest based on average metabolic change vector loadings (Table 2) with corresponding false discovery rate corrected  $p$ -values from paired  $t$  tests. Boxes indicate the group interquartile range (IQR), and the horizontal line within each box indicates the group median. Whiskers extend above and below the upper and lower boundary of

the boxes to the group maximum and minimum (up to  $1.5 \times \text{IQR}$ ), respectively. Relative intensities for the individual samples in each group are shown as the points overlapping with the boxplots. Features are listed in descending  $^1\text{H}$  nuclear magnetic resonance (NMR) chemical shift (ppm) order. Corresponding overlapped  $^1\text{H}$  NMR spectra for these features are shown in Fig. S10

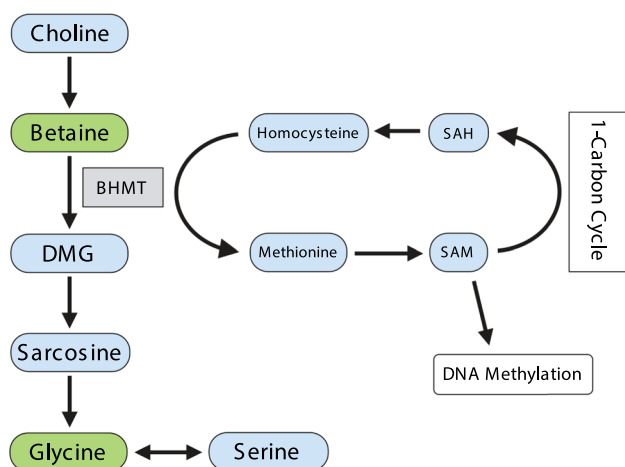


**Fig. 5** Flowchart showing selected reactions relating to glycine and serine metabolism, focusing on the oxidation of choline to glycine. Black arrows indicate metabolic reactions; blue ovals indicate specified metabolites; and green ovals indicate metabolites with decreased abundance in growth anomaly relative to unaffected samples. Gray box indicates the enzyme betaine–homocysteine S-methyltransferase (BHMT), which is responsible for catalyzing the conversion of betaine and homocysteine to dimethylglycine and methionine. DMG = Dimethylglycine; SAM = S-adenosylmethionine; and SAH = S-adenosylhomocysteine

benign), the carcinogenic potential of this pathway in coral GAs warrants further investigation. Based on these untargeted results, we hypothesize that heterotrophic feeding, the oxidation of choline to glycine, glycine levels in the skeletal organic matrix, and epigenetic DNA methylation are decreased in GA lesions relative to surrounding unaffected tissues. We further theorize that these are concurrent results related to GA formation and/or growth rather than mutually exclusive GA processes. Therefore, metabolites belonging to these pathways are of interest for GA pathophysiology going forward and could be the focus of future validation and targeted studies to further elucidate GA impacts.

### Wider GA pathophysiology perspectives

Our study is the first application of untargeted metabolomics analyses to study coral disease in situ and thus offers a unique perspective into the biochemical impacts of GAs in *P. compressa*. These results are a part of a larger investigation of GA pathophysiology that includes morphological descriptions and skeletal trace element measurements of these same coral samples. Elemental and

morphological results showed decreased pH of GA calcifying fluid and a porous and fragile GA skeleton, respectively, which we theorized to be the result of energy reallocation away from internal pH regulation to facilitate elevated GA tissue growth (Andersson et al. 2020). Our metabolomics results expand on these findings by providing additional demonstrations of abnormal energetics (i.e., increased unaffected and GA extract yield, metabolomic profile differences between unaffected–GA samples) and by identifying specific metabolites and metabolic pathways of interest that may be altered in this irregular GA metabolism. Combined results from these studies seemingly indicate that GA metabolism is unbalanced toward promoting rapid lesion growth, often at the expense of other essential biological processes and the surrounding unaffected tissues, despite evidence that traditional autotrophic and heterotrophic energy sources are compromised in GAs. Both studies also demonstrate the utility of analyzing paired GA and unaffected samples when studying GAs. Overall, this work broadly advances our understanding of GA pathophysiology, particularly in *P. compressa*. Further work on GAs could aim to validate metabolomics results with targeted measurements of important metabolites and to extend GA characterization to additional analytical methods (e.g., mass spectrometry-based metabolomics, transcriptomics, stable isotope analyses to assess heterotrophic nutrition, DNA methylation assays, 16S rRNA gene sequencing) to provide a more comprehensive comparison of diseased and healthy holobiont functioning.

**Acknowledgements** We thank the Woodley lab staff at the National Oceanic and Atmospheric Administration coral culture facility for providing *Orbicella faveolata* specimens for use as control materials in this work. We also thank the National Institute of Standards and Technology Biorepository for storage of the coral samples, Ben Flanagan for his help with laboratory work, and Julie Loewenstein for her advice in preparing this manuscript. Diagrams used in Figs. 1a and 5 were created using BioRender scientific illustration tool (Biorender.com). *P. compressa* illustrations used in Fig. 1a are based on a photograph by David R. with modifications (<https://www.inaturalist.org/observations/14939424>). Observation © David R. 2018 (Creative Commons Attribution-NonCommercial license (CC BY-NC 4.0)).

## Declarations

**Conflict of interest** On behalf of all authors, the corresponding author states that there is no conflict of interest. Certain commercial equipment, instruments, or materials are identified in this paper to specify the experimental procedure adequately. Such identification is not intended to imply recommendation or endorsement by the National Institute of Standards and Technology and the U.S. Government, nor is it intended to imply that the materials or equipment identified is necessarily the best available for the purpose.

## References

- Aeby GS, Williams GJ, Franklin EC, Kenyon J, Cox EF, Coles S, Work TM (2011a) Patterns of coral disease across the Hawaiian Archipelago: Relating disease to environment. *PLoS One* 6:e20370
- Aeby GS, Williams GJ, Franklin EC, Haapkyla J, Harvell CD, Neale S, Page CA, Raymundo L, Vargas-Ángel B, Willis BL, Work TM, Davy SK (2011b) Growth anomalies on the coral genera *Acropora* and *Porites* are strongly associated with host density and human population size across the Indo-Pacific. *PLoS One* 6:e16887
- Alonso A, Marsal S, Julià A (2015) Analytical methods in untargeted metabolomics: State of the art in 2015. *Front Bioeng Biotechnol* 3:23
- Amelio I, Cutruzzolà F, Antonov A, Agostini M, Melino G (2014) Serine and glycine metabolism in cancer. *Trends Biochem Sci* 39:191–198
- Andersson ER, Day RD, Loewenstein JM, Woodley CM, Schock TB (2019) Evaluation of sample preparation methods for the analysis of reef-building corals using <sup>1</sup>H-NMR-based metabolomics. *Metabolites* 9:32
- Andersson ER, Stewart JA, Work TM, Woodley CM, Schock TB, Day RD (2020) Morphological, elemental, and boron isotopic insights into pathophysiology of diseased coral growth anomalies. *Sci Rep* 10:8252
- Aronson RB, Precht WF (2001) White-band disease and the changing face of Caribbean coral reefs. *Hydrobiologia* 460:25–38
- Ashraf M, Foolad MR (2007) Roles of glycine betaine and proline in improving plant abiotic stress resistance. *Environ Exp Bot* 59:206–216
- Bahr KD, Jokiel PL, Toonen RJ (2015) The unnatural history of Kāneʻohe bay: Coral reef resilience in the face of centuries of anthropogenic impacts. *PeerJ* 3:e950
- Benjamini Y, Hochberg Y (1995) Controlling the False Discovery Rate: A Practical and Powerful Approach to Multiple Testing. *J R Stat Soc Ser B* 57:289–300
- Bijlsma S, Bobeldijk I, Verheij ER, Ramaker R, Kochhar S, Macdonald IA, Van Ommen B, Smilde AK (2006) Large-scale human metabolomics studies: A strategy for data (pre-) processing and validation. *Anal Chem* 78:567–574
- Bligh EG, Dyer WJ (1959) A rapid method of total lipid extraction and purification. *Can J of Biochem Physiol* 37:911–917
- Bruckner AW (2016) History of coral disease research. In: *Diseases of coral*. John Wiley and Sons Inc, pp 52–84
- Bundy JG, Davey MP, Viant MR (2009) Environmental metabolomics: A critical review and future perspectives. *Metabolomics* 5:3–21
- Burge CA, Mark Eakin C, Friedman CS, Froelich B, Hershberger PK, Hofmann EE, Petes LE, Prager KC, Weil E, Willis BL, Ford SE, Harvell CD (2014) Climate Change Influences on Marine Infectious Diseases: Implications for Management and Society. *Ann Rev Mar Sci* 6:249–277
- Burns JHR, Takabayashi M (2011) Histopathology of growth anomaly affecting the coral, *Montipora capitata*: Implications on biological functions and population viability. *PLoS One* 6:e28854
- Burriesci MS, Raab TK, Pringle JR (2012) Evidence that glucose is the major transferred metabolite in dinoflagellate-cnidarian symbiosis. *J Exp Biol* 215:3467–3477
- Cappello T, Mauceri A, Corsaro C, Maisano M, Parrino V, Lo Paro G, Messina G, Fasulo S (2013) Impact of environmental pollution on caged mussels *Mytilus galloprovincialis* using NMR-based metabolomics. *Mar Pollut Bull* 77:132–139

- Coles SL, Seapy DG (1998) Ultra-violet absorbing compounds and tumorous growths on acroporid corals from Bandar Khayran, Gulf of Oman, Indian Ocean. *Coral Reefs* 17:195–198
- Cui G, Liew YJ, Li Y, Kharbatia N, Zahran NI, Emwas A-H, Eguiluz VM, Aranda M (2019) Host-dependent nitrogen recycling as a mechanism of symbiont control in *Aiptasia*. *PLOS Genet* 15:e1008189
- De Meyer T, Sinnaeve D, Van Gasse B, Tsiporkova E, Rietzschel ER, De Buyzere ML, Gillebert TC, Bekaert S, Martins JC, Van Criekeinghe W (2008) NMR-based characterization of metabolic alterations in hypertension using an adaptive, intelligent binning algorithm. *Anal Chem* 80:3783–3790
- Domart-Coulon IJ, Traylor-Knowles N, Peters E, Elbert D, Downs CA, Price K, Stubbs J, McLaughlin S, Cox E, Aeby G, Brown PR, Ostrander GK (2006) Comprehensive characterization of skeletal tissue growth anomalies of the finger coral *Porites compressa*. *Coral Reefs* 25:531–543
- Frazier M, Helmkampf M, Bellinger MR, Geib SM, Takabayashi M (2017) De novo metatranscriptome assembly and coral gene expression profile of *Montipora capitata* with growth anomaly. *BMC Genomics* 18:710
- Goodacre R (2007) Metabolomics of a Superorganism. *J Nutr* 137:259S–266S
- Gordon B.R, Laggat W, Motti CA (2013) Extraction protocol for nontargeted NMR and LC-MS metabolomics-based analysis of hard coral and their algal symbionts. In: *Metabolomics tools for natural product discovery: methods and protocols*. Humana Press, pp 129–147
- Green EP, Bruckner AW (2000) The significance of coral disease epizootiology for coral reef conservation. *Biol Conserv* 96:347–361
- Grottoli AG, Rodrigues LJ, Palardy JE (2006) Heterotrophic plasticity and resilience in bleached corals. *Nature* 440:1186–1189
- Hadaidi G, Gegner HM, Ziegler M, Voolstra CR (2019) Carbohydrate composition of mucus from scleractinian corals from the central Red Sea. *Coral Reefs* 38:21–27
- Hagedorn M, Carter V, Zuchowicz N, Phillips M, Penfield C, Shamenek B, Vallen EA, Kleinhans FW, Peterson K, White M, Yancey PH (2015) Trehalose is a chemical attractant in the establishment of coral symbiosis. *PLoS One* 10: e0117087
- Hartmann AC, Petras D, Quinn RA, Protsyuk I, Archer FI, Ransome E, Williams GJ, Bailey BA, Vermeij MJA, Alexandrov T, Dorrestein PC, Rohwer FL (2017) Meta-mass shift chemical profiling of metabolomes from coral reefs. *Proc Natl Acad Sci USA* 114:11685–11690
- Hillyer KE, Dias D, Lutz A, Roessner U, Davy SK (2018) <sup>13</sup>C metabolomics reveals widespread change in carbon fate during coral bleaching. *Metabolomics* 14:12
- Hillyer KE, Dias DA, Lutz A, Wilkinson SP, Roessner U, Davy SK (2017) Metabolite profiling of symbiont and host during thermal stress and bleaching in the coral *Acropora aspera*. *Coral Reefs* 36:105–118
- Hoegh-Guldberg O, Mumby PJ, Hooten AJ, Steneck RS, Greenfield P, Gomez E, Harvell CD, Sale PF, Edwards AJ, Caldeira K, Knowlton N, Eakin CM, Iglesias-Prieto R, Muthiga N, Bradbury RH, Dubi A, Hatzitolos ME (2007) Coral reefs under rapid climate change and ocean acidification. *Science* 318:1737–1742
- Hughes TP, Barnes ML, Bellwood DR, Cinner JE, Cumming GS, Jackson JBC, Kleypas J, Van De Leemput IA, Lough JM, Morrison TH, Palumbi SR, Van Nes EH, Scheffer M (2017) Coral reefs in the Anthropocene. *Nature* 546:82–90
- Jacob D, Deborde C, Lefebvre M, Maucourt M, Moing A (2017) NMRProcFlow: a graphical and interactive tool dedicated to 1D spectra processing for NMR-based metabolomics. *Metabolomics* 13:36
- Joyce AR, Palsson B (2006) The model organism as a system: Integrating “omics” data sets. *Nat Rev Mol Cell Biol* 7:198–210
- Kaczmarek L, Richardson LL (2007) Transmission of growth anomalies between Indo-Pacific *Porites* corals. *J Invertebr Pathol* 94:218–221
- Kell DB, Oliver SG (2004) Here is the evidence, now what is the hypothesis? The complementary roles of inductive and hypothesis-driven science in the post-genomic era. *BioEssays* 26:99–105
- Kelly LA, Heintz T, Lamb JB, Ainsworth TD, Willis BL (2016) Ecology and pathology of novel plaque-like growth anomalies affecting a reef-building coral on the great barrier reef. *Front Mar Sci* 3:151
- Knowlton N (2001) The future of coral reefs. *Proc Natl Acad Sci USA* 98:5419–5425
- Lesser MP, Bythell JC, Gates RD, Johnstone RW, Hoegh-Guldberg O (2007) Are infectious diseases really killing corals? Alternative interpretations of the experimental and ecological data. *J Exp Mar Bio Ecol* 346:36–44
- Liu X, Zhang L, You L, Yu J, Cong M, Wang Q, Li F, Li L, Zhao J, Li C, Wu H (2011) Assessment of clam *Ruditapes philippinarum* as heavy metal bioindicators using NMR-based metabolomics. *Clean - Soil, Air, Water* 39:759–766
- Lohr KE, Camp EF, Kuzhiumparambil U, Lutz A, Leggat W, Patterson JT, Suggett DJ (2019a) Resolving coral photoacclimation dynamics through coupled photophysiological and metabolomic profiling. *J Exp Biol* 222:jeb195982
- Lohr KE, Khattri RB, Guingab-Cagmat J, Camp EF, Merritt ME, Garrett TJ, Patterson JT (2019b) Metabolomic profiles differ among unique genotypes of a threatened Caribbean coral. *Sci Rep* 9:6067
- Madsen EL (2005) Identifying microorganisms responsible for ecologically significant biogeochemical processes. *Nat Rev Microbiol* 3:439–446
- Markley JL, Brüschweiler R, Edison AS, Eghbalnia HR, Powers R, Raftery D, Wishart DS (2017) The future of NMR-based metabolomics. *Curr Opin Biotechnol* 43:34–40
- Matthews JL, Cuning R, Ritson-Williams R, Oakley CA, Lutz A, Roessner U, Grossman AR, Weis VM, Gates RD, Davy SK (2020) Metabolite pools of the reef building coral *Montipora capitata* are unaffected by Symbiodiniaceae community composition. *Coral Reefs* 39:1727–1737
- Moberg F, Folke C (1999) Ecological goods and services of coral reef ecosystems. *Ecol Econ* 29:215–233
- Nakae D, Yoshiji H, Mizumoto Y, Horiguchi K, Shiraiwa K, Tamura K, Denda A, Konishi Y (1992) High Incidence of Hepatocellular Carcinomas Induced by a Choline Deficient L-Amino Acid Defined Diet in Rats. *Cancer Res* 52:5042–5045
- Niculescu MD, Zeisel SH (2002) Diet, methyl donors and DNA methylation: interactions between dietary folate, methionine and choline. *J Nutr* 132:2333S–2335S
- Ochsenkühn MA, Röthig T, D’Angelo C, Wiedenmann J, Voolstra CR (2017) The role of floridoside in osmoadaptation of coral-associated algal endosymbionts to high-salinity conditions. *Sci Adv* 3:e1602047
- Odum HT, Odum EP (1955) Trophic structure and productivity of a windward coral reef community on Eniwetok Atoll. *Ecol Monogr* 25:291–320
- Palmer CV, Baird AH (2018) Coral tumor-like growth anomalies induce an immune response and reduce fecundity. *Dis Aquat Organ* 130:77–81
- Parkinson JE, Baums IB (2014) The extended phenotypes of marine symbioses: Ecological and evolutionary consequences of intraspecific genetic diversity in coral-algal associations. *Front Microbiol* 5:445

- Pollock FJ, Morris PJ, Willis BL, Bourne DG (2011) The urgent need for robust coral disease diagnostics. *PLoS Pathog* 7:e1002183
- Preston S, Richards Z (2021) Biological consequences of an outbreak of growth anomalies on *Isopora palifera* at the Cocos (Keeling) Islands. *Coral Reefs* 40:97–109
- Putnam HM, Davidson JM, Gates RD (2016) Ocean acidification influences host DNA methylation and phenotypic plasticity in environmentally susceptible corals. *Evol Appl* 9:1165–1178
- Puverel S, Tambutté E, Pereira-Mouriès L, Zoccola D, Allemand D, Tambutté S (2005) Soluble organic matrix of two Scleractinian corals: Partial and comparative analysis. *Comp Biochem Physiol - B Biochem Mol Biol* 141:480–487
- Quinn RA, Vermeij MJA, Hartmann AC, d'Auriac IG, Benler S, Haas A, Quistad SD, Lim YW, Little M, Sandin S, Smith JE, Dorrestein PC, Rohwer F (2016) Metabolomics of reef benthic interactions reveals a bioactive lipid involved in coral defence. *Proc R Soc B Biol Sci* 283:20160469
- Roach TNF, Little M, Arts MGI, Huckeba J, Haas AF, George EE, Quinn RA, Cobián-Güemes AG, Naliboff DS, Silveira CB, Vermeij MJA, Kelly LW, Dorrestein PC, Rohwer F (2020) A multiomic analysis of in situ coral-turf algal interactions. *Proc Natl Acad Sci USA* 117:13588–13595
- Roach TNF, Dilworth J, Christian Martin H, Jones AD, Quinn RA, Drury C (2021) Metabolomic signatures of coral bleaching history. *Nat Ecol Evol*
- Roberts LD, Souca AL, Gerszten RE, Clish CB (2012) Targeted metabolomics. In: *Current protocols in molecular biology*. John Wiley and Sons Inc, 98:30.2:30.2.1–30.2.24
- Ross A, Schlotterbeck G, Dieterle F, Senn H (2007) NMR spectroscopy techniques for application to metabolomics. In: *The handbook of metabolomics and metabolomics*. Elsevier, pp 55–108
- Sale TL, Hunter CL, Hong C, Moran AL (2019) Morphology, lipid composition, and reproduction in growth anomalies of the reef-building coral *Porites evermanni* and *Porites lobata*. *Coral Reefs* 38:881–893
- Sogin EM, Putnam HM, Anderson PE, Gates RD (2016) Metabolomic signatures of increases in temperature and ocean acidification from the reef-building coral, *Pocillopora damicornis*. *Metabolomics* 12:71
- Sogin EM, Anderson P, Williams P, Chen CS, Gates RD (2014) Application of <sup>1</sup>H-NMR metabolomic profiling for reef-building corals. *PLoS One* 9:e111274
- Sogin EM, Putnam HM, Nelson CE, Anderson P, Gates RD (2017) Correspondence of coral holobiont metabolome with symbiotic bacteria, archaea and Symbiodinium communities. *Environ Microbiol Rep* 9:310–315
- Southam AD, Easton JM, Stentiford GD, Ludwig C, Arvanitis TN, Viant MR (2008) Metabolic changes in flatfish hepatic tumours revealed by NMR-based metabolomics and metabolic correlation networks. *J Proteome Res* 7:5277–5285
- Spies NP, Takabayashi M (2013) Expression of galaxin and oncogene homologs in growth anomaly in the coral *Montipora capitata*. *Dis Aquat Organ* 104:249–256
- Stien D, Suzuki M, Rodrigues AMS, Yvin M, Clergeaud F, Thorel E, Lebaron P (2020) A unique approach to monitor stress in coral exposed to emerging pollutants. *Sci Rep* 10:9601
- Stien D, Clergeaud F, Rodrigues AMS, Lebaron K, Pillot R, Romans P, Fagervold S, Lebaron P (2019) Metabolomics reveal that octocrylene accumulates in *Pocillopora damicornis* tissues as fatty acid conjugates and triggers coral cell mitochondrial dysfunction. *Anal Chem* 91:990–995
- Stimson J (2011) Ecological characterization of coral growth anomalies on *Porites compressa* in Hawai'i. *Coral Reefs* 30:133–142
- Sumner LW, Amberg A, Barrett D, Beale MH, Beger R, Daykin CA, Fan TWM, Fiehn O, Goodacre R, Griffin JL, Hankemeier T, Hardy N, Harnly J, Higgashi R, Kopka J, Lane AN, Lindon JC, Marriott P, Nicholls AW, Reily MD, Thaden JJ, Viant MR (2007) Proposed minimum reporting standards for chemical analysis: Chemical Analysis Working Group (CAWG) Metabolomics Standards Initiative (MSI). *Metabolomics* 3:211–221
- Szymańska E, Saccenti E, Smilde AK, Westerhuis JA (2012) Double-check: validation of diagnostic statistics for PLS-DA models in metabolomics studies. *Metabolomics* 8:3–16
- Ulrich EL, Akutsu H, Doreleijers JF, Harano Y, Ioannidis YE, Lin J, Livny M, Mading S, Maziuk D, Miller Z, Nakatani E, Schulte CF, Tolmie DE, Kent Wenger R, Yao H, Markley JL (2008) BioMagResBank. *Nucleic Acids Res* 36:D402–D408
- van Dam J. W., Negri A. P., Uthicke S., and Mueller J. F. (2011) Chemical pollution of coral reefs: exposure and ecological effects. In: *Ecological impacts of toxic chemicals*. Bentham Science Publisher Ltd, pp 187–211
- van den Berg RA, Hoefsloot HCJ, Westerhuis JA, Smilde AK, van der Werf MJ (2006) Centering, scaling, and transformations: Improving the biological information content of metabolomics data. *BMC Genomics* 7:142
- Viant MR (2008) Recent developments in environmental metabolomics. *Mol Biosyst* 4:980–986
- Vohsen SA, Fisher CR, Baums IB (2019) Metabolomic richness and fingerprints of deep-sea coral species and populations. *Metabolomics* 15:34
- Williams A, Chiles EN, Conetta D, Pathmanathan JS, Cleves PA, Putnam HM, Su X, Bhattacharya D (2021) Metabolomic shifts associated with heat stress in coral holobionts. *Sci Adv* 7:eabd4210
- Wishart DS, Tzur D, Knox C, Eisner R, Guo AC, Young N, Cheng D, Jewell K, Arndt D, Sawhney S, Fung C, Nikolai L, Lewis M, Coutouly MA, Forsythe I, Tang P, Shrivastava S, Jeroncic K, Stothard P, Amegbey G, Block D, Hau DD, Wagner J, Miniaci J, Clements M, Gebremedhin M, Guo N, Zhang Y, Duggan GE, MacInnis GD, Weljie AM, Dowlatbadi R, Bamforth F, Clive D, Greiner R, Li L, Marrie T, Sykes BD, Vogel HJ, Querengesser L (2007) HMDB: The human metabolome database. *Nucleic Acids Res* 35:D521–D526
- Work TM, Aeby GS (2006) Systematically describing gross lesions in corals. *Dis Aquat Organ* 70:155–160
- Work TM, Kaczmarek LT, Peters EC (2016) Skeletal growth anomalies in corals. In: *Diseases of coral*. John Wiley and Sons Inc, pp 291–299
- Wu H, Southam AD, Hines A, Viant MR (2008) High-throughput tissue extraction protocol for NMR- and MS-based metabolomics. *Anal Biochem* 372:204–212
- Xia J, Wishart DS (2016) Using metaboanalyst 3.0 for comprehensive metabolomics data analysis. *Curr Protoc Bioinform* 55:14.10.1–14.10.91
- Yasuda N, Hidaka M (2012) Cellular kinetics in growth anomalies of the scleractinian corals *Porites australiensis* and *Montipora informis*. *Dis Aquat Organ* 102: 1–11
- Zhang Y, Sun J, Mu H, Lun JCY, Qiu JW (2017) Molecular pathology of skeletal growth anomalies in the brain coral *Platygyra carmosa*: A meta-transcriptomic analysis. *Mar Pollut Bull* 124:660–667

**Publisher's Note** Springer Nature remains neutral with regard to jurisdictional claims in published maps and institutional affiliations.